Highly Porous and Drug-Loaded Amorphous Solid Dispersion Microfiber Scaffolds of Indomethacin Prepared by Melt Electrowriting

Kessler, Larissa

2023-01-13

Kessler , L , Mirzaei , Z , Kade , J C & Luxenhofer , R 2023 , ' Highly Porous and Drug-Loaded Amorphous Solid Dispersion Microfiber Scaffolds of Indomethacin Prepared by Melt Electrowriting ' , ACS applied polymer materials , vol. 5 , no. 1 , pp. 913-922 . https://doi.org/10.1021/acsapm.2c

http://hdl.handle.net/10138/356730
https://doi.org/10.1021/acsapm.2c01845

ACS APPLIED POLYMER MATERIALS

pubs.acs.org/acsapm

Article

Highly Porous and Drug-Loaded Amorphous Solid Dispersion Microfiber Scaffolds of Indomethacin Prepared by Melt Electrowriting

Larissa Keßler, Zeynab Mirzaei, Juliane C. Kade, and Robert Luxenhofer*

Cite This: *ACS Appl. Polym. Mater.* 2023, 5, 913–922

Read Online

ACCESS | Metrics & More | Article Recommendations | Supporting Information

ABSTRACT: Melt electrowriting (MEW) is an additive manufacturing technology enabling the production of highly porous microfiber scaffolds, suggested in particular for use in biomedical applications, including drug delivery. Indomethacin (IND) is a nonselective anti-inflammatory drug, for which sublingual delivery could offer advantages such as rapid absorption by the veins in the mouth floor while overcoming the side effects of peroral delivery such as damage to the gastrointestinal mucosa barrier. This study introduces MEW as a processing method to obtain rapid-dissolving drug-releasing scaffolds, containing IND as a model drug, for sublingual drug delivery applications. For this, an amorphous solid dispersion (ASD) of IND in combination with a poly(2-oxazoline)-based amphiphilic triblock copolymer excipient is introduced, enabling ultra-high drug loading. We prepared highly porous, melt electrowritten drug-loaded scaffolds with different polymer/IND w/w ratios up to 1:2 and assessed their morphology, amorphicity, and IND release rate. The results show completely amorphous dispersion of the polymer and drug after MEW processing resulting in smooth and uniform fibers and rapid dissolution of the drug-loaded scaffold. These first water-soluble melt electrowritten IND-loaded microfiber scaffolds break ground as a model for rapid sublingual delivery of ultra-high drug-loaded ASDs.

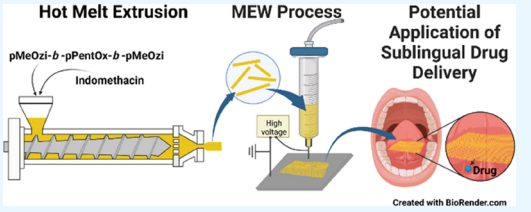

KEYWORDS: *amphiphilic block copolymer, poly(2-oxazoline), poly(2-oxazine), drug formulation, electrohydrodynamic direct writing*

1. INTRODUCTION

Sublingual or buccal drug delivery approaches have gained increasing attention due to the fast and direct drug uptake in the oral cavity. The sublingual route is known to be one of the most effective ones, as the drug is directly absorbed by the high number of capillaries below the tongue and effectively brought to the blood circulation.[1,2] Additionally, sublingual drug-delivery systems are designed for the drug to avoid passing the gastrointestinal tract, reducing potential side effects of the drugs observed with common peroral delivery, such as gastrointestinal ulceration, and limitations of local acidic conditions, as well as enzymatic degradation.[3] Furthermore, these approaches simplify the uptake of the drugs, as they avoid potential swallowing difficulties,[4] improving patient compliance.

Indomethacin (IND) is used here as a model drug for the development of novel sublingual drug delivery approaches. This nonsteroidal anti-inflammatory drug is commonly used as a painkiller by oral administration to reduce fever and swelling, as well as a medication to treat rheumatoid arthritis or osteoarthritis due to its strong action and high therapeutic efficacy.[5] However, at the same time, its short half-life time and the associated repeated oral administration result in toxicity issues in the digestive system and kidneys as well as malaises like nausea, stomach pain, and diarrhea, which could be expected to be reduced by using a sublingual delivery system.[6]

Maintaining drugs in their amorphous state improves the dissolution rate and oral bioavailability.[7] However, some limitations including recrystallization due to the physical instability of the amorphous state and residual micro-crystallinity of the drug can cause problems such as patient-to-patient variability.[8] This can be addressed and overcome via preparation of amorphous solid dispersions (ASDs) using suitable excipients, e.g., through tuning the interactions between polymeric excipients and drugs.[9] One well-known and widely used method to fabricate ASDs is hot melt extrusion (HME). This method involves melting and intensive mixing of the drug into the polymer matrix, resulting in the formation of a single phase.[10] There are numerous well-known and well-studied polymer excipients for the preparation of ASDs.[11] Recently, poly(2-ethyl-2-oxazoline) has been investigated in this context[12] and compared to the structurally similar poly(vinyl pyrrolidone), with the former showing a better performance.[13] The selection of an excipient is not only

Received: October 22, 2022
Accepted: December 20, 2022
Published: January 3, 2023

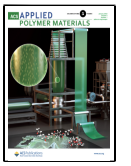

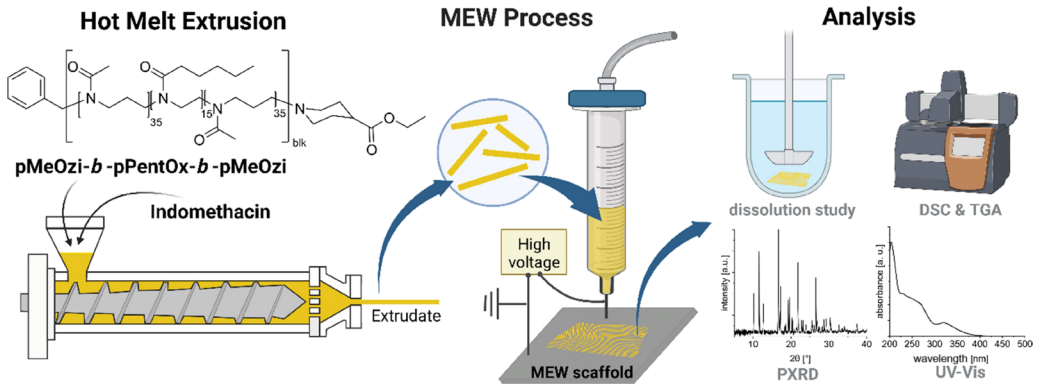

Figure 1. Schematic overview of this study. Blending of the triblock copolymer with indomethacin via hot melt extrusion and subsequent processing into 3D porous scaffolds using melt electrowriting for potential sublingual drug-delivery applications. Created with biorender.com.

based on the processability using a given method and the possibility of designing a controlled release from the amorphous formulation, but also the miscibility and possible interactions between the drug and polymer play an important role.[14]

Previously, poly(2-oxazoline)/poly(2-oxazine) triblock copolymers have been employed very successfully in high drug loading formulations[15,16] with up to and more than 50 wt% of the drug for a variety of drugs.[17−19] In addition, diblock, random, and gradient copolymers from poly(2-oxazoline)s/poly(2-oxazine)s have been investigated as potential excipients[20−22] and some systems also allowed high drug loadings.[23−25]

Depending on the properties of the chosen polymer and drug, the drug loading capacity can be changed and adjusted to the required needs.[26] An amorphous blend facilitates a faster dissolution and drug release compared to crystalline drug-loaded material, due to its higher free energy[27] achievable for example using melt processing techniques such as previously mentioned HME. Furthermore, drug delivery systems with a high surface area to volume ratio are also beneficial, as they can provide a high capacity of drug loading in addition to a fast dissolution due to their highly porous design.[28] Solution electrospun fibers containing drugs are already well studied as fast sublingual drug delivery systems due to their high surface area and exceedingly small fiber diameters showing great potential for this application.[2] In addition, they provide faster dissolution compared to films; however, the electrospinning technique requires (often toxic) solvents, and the processed fibers are randomly oriented,[29] limiting the degree of control over the morphology. Another method capable of producing fibers within the lower micron range is called melt electrowriting (MEW), which electrostatically draws a polymer melt out of a syringe onto a computer-controlled moving collector without the need of (toxic) solvents.[30] MEW is a high-resolution additive manufacturing technology allowing accurate microfiber placement with fiber diameters commonly ranging between 5 and ∼50 μm and production of unique printing patterns, as well as highly porous microfiber scaffolds.[31,32] This technique uniquely fills the fabrication gap between solution electrospinning (SES) and/or electrohydrodynamic jet writing on the one hand and melt extrusion-based direct writing on the other.[33] The former two techniques produce sub-micron fibers with either chaotic and uncontrollable fiber placement for SES or controlled fiber placement when using electrohydrodynamic jet writing commonly based on polymer solutions, while melt extrusion-based direct writing allows good fiber placement but generates larger diameters, typically well of above 100 μm.[34] The high porosity and larger surface area of the MEW scaffolds compared to films or other 3D printed constructs benefit the use in a variety of biomedical applications, including tissue engineering[35−37] and drug delivery.[36,38]

In this study, an amphiphilic triblock copolymer (pMeOzi-*b*-pPentOx-*b*-pMeOzi) has been synthesized and explored as an excipient to enable (I) processing via HME and MEW, (II) retaining the fully amorphous character of the drug, and (III) allowing fast and complete dissolution of the incorporated drug (Figure 1).

For this purpose, pMeOzi-*b*-pPentOx-*b*-pMeOzi has been blended via HME with different ratios of IND, before these blends were processed using MEW for the first time (Figure 1). Furthermore, the influence of the drug-loading content on the processability was elucidated, and the blends and resulting drug-loaded fibrous scaffolds were investigated regarding their properties using scanning electron microscopy (SEM), thermogravimetric analysis (TGA), differential scanning calorimetry (DSC), and powder X-ray diffraction (PXRD), as well as drug-release tests.

2. MATERIALS AND METHODS

2.1. Source of Materials. IND and benzylbromide were purchased from TCI chemicals (Zwijndrecht, Belgium), and 3-amino-propanol, 2-amino-ethanol, acetonitrile, benzonitrile, CaH_2, and zinc acetate dihydrate were obtained from Sigma-Aldrich (Helsinki, Finland) and used as received unless otherwise stated.

2-Methyl-2-oxazine and 2-pentyl-2-oxazoline were dried by refluxing over CaH_2 under an inert atmosphere, followed by distillation prior to use. Benzonitrile was dried by refluxing over P_2O_5 under an inert atmosphere, followed by distillation prior to use.

2.2. Synthesis of the Polymer. The monomers 2-methyl-2-oxazine (MeOzi) and 2-pentyl-2-oxazoline (PentOx) were synthesized following the procedure by Witte and Seeliger.[39] Detailed information on the synthesis can be found in the Supporting Information (Tables S1, S2 and Figure S1, S2). Briefly explained, the respective nitrile, 3-amino-propanol for the synthesis of the 2-oxazines or 2-amino-ethanol for the synthesis of the 2-oxazolines, and catalytic amounts of zinc acetate dihydrate were mixed in a N_2 flushed flask and heated to 130 °C under reflux for 2 days. The progress was controlled by ^{1}H NMR spectroscopy. After completion of the reaction, the reaction mixture was dissolved in dichloromethane and washed with H_2O three times. The organic phase was dried with Na_2SO_4 and concentrated. The raw product was dried over CaH_2 and distilled under reduced pressure under a N_2 atmosphere to yield the

https://doi.org/10.1021/acsapm.2c01845
ACS Appl. Polym. Mater. 2023, 5, 913−922

Table 1. MEW Printing Parameters for the Neat Polymer and Different Polymer/IND Ratios

	$T_{syringe}$[°C]	T_{nozzle}[°C]	voltage [kV]	pressure [MPa]	distance [mm]	speed [mm min^{-1}]
polymer/IND w/w 1:0	155	155	3.0−4.0	0.1	4	1500
polymer/IND w/w 2:1	140	140	2.5−3.0	0.1	4	1400
polymer/IND w/w 1:1	135	135	3.0−5.5	0.1	4	1000
polymer/IND w/w 1:2	130	130	2.5−4.5	0.1	4	700

product as a colorless liquid. MeOzi was distilled directly out of the reaction mixture after completion of the reaction.

The polymer synthesis and workup procedures were carried out as described elsewhere.[40] Briefly, the initiator was added to a dried and N_2-flushed Schlenk flask and dissolved in the respective amount of solvent. The monomer MeOzi was added, and the reaction mixture was heated to 130 °C and stirred until complete consumption of the monomer, as was monitored by ^{1}H NMR spectroscopy. After consumption of MeOzi, the mixture was cooled to room temperature and the second block, PentOx, was added. The mixture was heated to 130 °C overnight. The same procedure was repeated for the third block MeOzi. After confirmation of monomer consumption by ^{1}H NMR, the polymerization was terminated by addition of ethyl-isonipecotate at 50 °C for 4 h. The solvent was removed under reduced pressure and the residue was transferred into a dialysis bag (MWCO 1 kDa, cellulose acetate) and dialyzed against deionized water for 2 days with several water changes. Afterward, the solution was recovered from the bag and lyophilized. More details regarding the synthesis can be found in the Supporting Information (Table S3 and Figure S3).

2.3. Hot Melt Extrusion (HME). HME was carried out on a ZE 9 HMI extruder (Three-Tec GmbH, Seon, Switzerland) at 100 °C in all three heating zones to ensure the formation of a continuous filament. The screw speed was set to 25 rpm for the whole extrusion process. The total amount of polymer and IND used for each round was about 5 g, which did not allow the use of continuous feeding. Therefore, manual feeding of the extruder had to be done to facilitate smooth, uniform, and nonsticky extrudates with improved handling under cooled storage conditions prior to use due to the low T_g of the polymer.

2.4. MEW Printing. A custom-built MEW printer similar to a previously described machine[41] was used in order to process the neat polymer and different ratios of polymer/IND extrudates into box structured scaffolds with dimensions of 24 × 24 mm^2 and 1 and 0.5 mm fiber spacing set within the G-code for polymer/IND and neat polymer scaffolds, respectively. The 3 mL glass syringes (Poulten & Graf GmbH, Germany) were loaded with different materials and heated for a minimum of 30 min prior to printing until the bubbles within the melt dissipated. For all experiments, a nozzle tip with an inner diameter of 0.337 mm (23G) was used and manually grinded to a length of 13 mm. Other applied printing parameters are listed in Table 1.

2.5. Characterization of the Extrudates and Scaffolds.

2.5.1. Thermogravimetric Analysis (TGA). TGA of the polymers was performed using a Netzsch STA 449 F3 Jupiter instrument (Germany) under a N_2 atmosphere. The samples of about 5 mg of neat polymers and polymer/IND w/w 1:1 extrudates were prepared in aluminum oxide crucibles heated to 140 °C (10 °C min^{-1}) and kept at constant temperature for 5 h and, then, further heated to 900 °C to detect the mass loss. The thermograms were evaluated using Origin software (OriginPro 2021. OriginLab Corp., Northampton, M.A.).

2.5.2. Differential Scanning Calorimetry (DSC). In order to evaluate the thermal behavior of neat IND, polymer/IND extrudates, and IND-loaded MEW-printed scaffolds, DSC was conducted using DSC Q 2000 (TA Instruments, USA). Specimens of about 5 mg of each sample were prepared in aluminum pans, sealed and heated from 5 to 200 °C, and subsequently cooled to −50 °C at a linear rate of 10 °C min^{-1} in a N_2 atmosphere. This cycle was repeated three times, i.e., heating to 200 °C and further cooling to −50 °C. In the final cycle, the samples were cooled from 200 °C to the room temperature, and the glass transition temperature (T_g), melting temperature (T_m), and enthalpy of fusion (ΔH_f) were determined. T_g was obtained from the inflection point of the second and third heating cycles, and T_m is the onset of the endothermic curve in the first heating. ΔH_f was calculated by determination of the area under the endotherm normalized to the mass of the polymer samples. The thermograms were evaluated using Origin software.

2.5.3. Powder X-ray Diffraction (PXRD). Diffraction patterns of neat IND and polymer/IND extrudates and scaffolds were obtained using an EMPYREAN X-ray diffractometer (Malvern PANalytical, Espoo, Finland) equipped with a transmission measurement geometry at room temperature and a voltage of 45 kV. Each sample was scanned between 5° and 40° 2θ with a step size of 0.013° 2θ and a step time of 49.47 s. The samples were ground, placed between two slices of Kapton tape and mounted on a transmission sample holder. The diffractograms were evaluated using Origin software.

2.5.4. Ultraviolet−Visible (UV−vis) Spectroscopy. UV−vis experiments were performed on a JASCO V-750 UV−vis spectrometer (JASCO UK Ltd., UK) equipped with a JASCO CTU-100 water-jacketed Peltier thermostat system at a wavelength of 320 nm and a temperature of 25 °C. A standard curve for IND was obtained by quantifying known amounts (Figure S4). Data were analyzed using the Origin software.

2.5.5. Rheology Characterization. Rheological properties of the polymer and polymer/IND extrudates were characterized using a Discovery Hybrid Rheometer HR-2 (TA Instruments, USA) equipped with an Environmental Test Chamber (ETC), and an air chiller system. The ETC is a high-temperature oven that provides uniform and stable temperature during the measurements. The samples were prepared in a hot air oven (Hewlett Packard HP 5890 Series, Gas Chromatograph, Agilent Technologies, USA) using in-house Teflon molds with a diameter of 25 mm. A plate−plate setup and an upper 25 mm plate were used for all the measurements. The behavior of the prepared samples was tested for 5 h under constant dynamic-mechanical low-shear conditions. The frequency was set to 10 rad s^{-1} and the shear strain to 1%. In the same measurement, the behavior of the complex viscosity during isothermal heating was observed. The temperature of the measurements was changed depending on the drug loading, to have similar temperatures to the MEW printing procedure. Data were analyzed using the Origin software.

2.5.6. Scanning Electron Microscopy (SEM). The diameter, morphology, and alignment of the MEW-processed fibers were characterized using field emission scanning electron microscopy (Hitachi S-4800, Hitachi Ltd., Japan). Before imaging, all samples were sputter coated with a thickness of 5 nm Au/Pd to create a conductive surface (Cressington 208HR, Ted Pella Inc., USA). An accelerating voltage of 5 kV was applied for imaging and ≈50 fibers were analyzed using ImageJ software[42] to determine the average fiber diameter for each sample. Furthermore, the heights of the scaffolds were calculated based on fiber diameter and the number of layers, and ≈10 pores were analyzed using ImageJ software[42] to report the average of real fiber spacing in both x and y directions for each scaffold, which is correlated with the pore size.

2.5.7. Dissolution Tests. Dissolution tests were performed on an in-house built Unites States Pharmacopeia dissolution apparatus 2 with a rotational speed of 50 rpm and temperature set to 37 °C. The dissolution medium was chosen to be 250 mL of phosphate-buffered saline (pH = 7.4) (Ph. Eur.). The printed scaffolds were weighed and added to the dissolution medium. At set time points between 0 an d 30 min, samples of 3 mL were removed, and the medium was

https://doi.org/10.1021/acsapm.2c01845
ACS Appl. Polym. Mater. 2023, 5, 913−922

refilled with 3 mL of fresh buffer solution (37 °C) every time. The amount of dissolved IND was determined by UV−vis spectroscopy at these time points. The data were evaluated using Origin software.

2.5.8. Size Exclusion Chromatography (SEC). SEC was measured with a Waters Acquity APC system, equipped with Acquity Column Manager—S, Sample Manager—pFTN, Isocratic Solvent Manager, Acquity RI Detector, and Acquity TUV Detector (Waters Corporation, USA). The used columns are Acquity APC XT 45, 125, and 200. Dimethylformamide (DMF, Fisher Scientific) was used as an eluent with a flow of 0.6 mL min^{-1} and at a temperature of 40 °C. The system was calibrated with poly(methyl methacrylate) (PMMA) standards (Polymer Standard Service). The data were analyzed using the software Empower 3 and Origin software.

2.5.9. Nuclear Magnetic Resonance Spectroscopy (NMR). ^{1}H NMR spectra were measured with an Avance III 500 MHz spectrometer from Bruker Biospin (Germany) at a temperature of 25 °C (298 K). The spectra were calibrated on the residual protonated solvent (CD_2Cl_2) signal (5.32 ppm). The data were evaluated using Bruker Topspin 4.1.3.

2.5.10. Glass Transition Predictions by the Gordon−Taylor Equation. The glass transition temperatures of homogeneous mixed ASD of the synthesized polymer and IND were calculated for different polymer/IND ratios ($T_g(x_{IND})$) using the Gordon−Taylor equation:

$$T_g(x_{IND}) = \frac{x_{IND}T_{g,IND} + K(1 - x_{IND})T_{g,Poly}}{x_{IND} + K(1 - x_{IND})} \quad (1)$$

with the glass transition of the neat polymer $T_{g,\,Poly}$ and neat IND $T_{g,\,IND}$, and the weight fraction of IND x_{IND}, respectively. The parameter K was calculated from eq 2 where $\Delta C_{p,\,Poly}$ and $\Delta C_{p,\,IND}$ are the amplitude of the C_p jump at the T_g determined for the neat polymer and the neat IND, respectively.

$$K = \frac{\Delta C_{p,Poly}}{\Delta C_{p,IND}} \quad (2)$$

3. RESULTS AND DISCUSSION

3.1. Synthesis and Characterization of the Polymer. The synthesis of the ABA triblock copolymer, comprising 2-methyl-2-oxazine (MeOzi) as block A and 2-pentyl-2-oxazoline (PentOx) as block B, was performed via living cationic ring-opening polymerization (LCROP), and the product was characterized by ^{1}H NMR spectroscopy and SEC (Figure S3A,B). During synthesis, a color change of the reaction mixture from colorless to orange was observed, suggesting some undesired side reactions. In addition, the required reaction time of the hydrophilic block was significantly longer than 2-methyl-2-oxazoline (MeOx), due to the lower reactivity of MeOzi.[43,44] Important to note, we used benzylbromide as an initiator, as the polymerization with the commonly used methyltriflate was not successful (no detailed analysis was conducted at this point). However, the change of the initiator coincided with a higher dispersity ($Đ$ = 1.45) than typically obtained for the LCROP. This notwithstanding, the thermal behavior of the polymer is crucial for the current contribution and was studied by DSC measurements. In the second heating cycle (Figure S3C), the polymer shows a T_g at 27 °C, crystallization at 56 °C, and T_m at 141 °C. The room-temperature PXRD pattern (of the unheated polymer) indicates the amorphous nature of the polymer. The DSC thermogram and PXRD pattern lead to the assumption that the first heating above 56 °C is necessary to induce partial crystallization of the polymer yielding a cold crystallization peak upon cooling and a T_m on second heating.

3.2. Preparation and Characterization of Polymer/IND Extrudates. Since the interest of this study was the fabrication of a (rapidly) dissolvable triblock polymer formulated with IND (Figure 1), blending of both components played a crucial role, especially in regard to obtain and retain both components in the amorphous state to favor a fast drug release and uptake.[26] For the blending process of the polymer and IND, manually grinding and mixing using a mortar was tested, but this proved impractical. The polymer was too viscous and sticky to allow effective blending. In contrast, the low T_g of the polymer makes it a good candidate for HME. Here, only a moderate temperature would be needed during the extrusion process so that the IND can be mixed in. The weight ratio between the polymer and IND can be easily altered by using different ratios of the respective compounds in the process.

As mentioned before, to reduce the applied heat as far as possible, the polymer and drug were extruded in different weight ratios using HME. Since the extrusion was done far below the T_m of IND (160 °C) and only for a brief time (approx. 10 min), some residual crystalline drug was still present and visible in the extrudates (Figure S5). This was also analyzed by DSC and PXRD analysis of the resulting extrudates. For this, the first heating cycle of the DSC was analyzed, which is usually not discussed due to the existence of polymer's thermal history that should be removed by heating.[45] However, in this study, the residual crystallinity of IND is only visible in the first heating curve of the DSC measurement because it has a very good glass stability (Class III compound)[46] and usually does not crystalize in the used DSC protocol. Furthermore, as the polymer and IND are heated higher than the extrusion temperature in the DSC run to reach the T_m of the drug, the solubility of the drug in the polymer matrix increases. If all of the drug gets solubilized while heating, no melting will be observed subsequently,[47] as observed for the samples with polymer/IND w/w ratios of 1:2 and 1:1 (Figure 2A). However, a residual broad endothermic

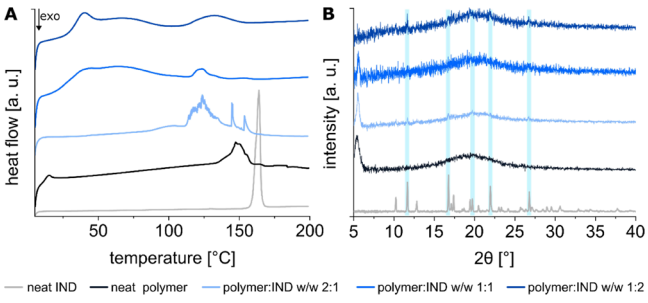

Figure 2. (A) First heating curves of the DSC measurements for IND and the polymer/IND extrudates with ratios (w/w) of 1:2, 1:1, and 2:1, respectively. (B) PXRD pattern of the neat IND and polymer, as well as the extrudates with different polymer/IND w/w ratios; 1:2, 1:1, and 2:1, respectively, measured at RT. Turquoise vertical lines highlight the residual crystallinity peaks.

transition between 110 and 140 °C can be observed for the sample containing a higher amount of polymer (polymer/IND w/w 2:1) followed by two sharp peaks at 145 and 153 °C.

To analyze the residual crystallinity of the samples without applying additional thermal energy, PXRD measurements of the extrudates were carried out (Figure 2B). The potential reflexes from residual crystallinity peaks are highlighted, and residual crystallinity is minute but not entirely absent, although it is difficult to accurately assign the peaks due to the low signal-to-noise ratio within the PXRD patterns.

https://doi.org/10.1021/acsapm.2c01845
ACS Appl. Polym. Mater. 2023, 5, 913−922

The resulting thermal properties of the neat polymer and the polymer/IND extrudates (Table 2) show a clear influence of drug loading on the T_g of the extrudates as it increases with higher drug concentration. Starting with a T_g of 27 °C for the neat polymer, the T_g values rise to 36 °C for the polymer/IND w/w 2:1, 37 °C for the polymer/IND w/w 1:1, and up to 42 and 43 °C for the polymer/IND w/w 1:2 and neat IND, respectively. The T_g for each sample was also calculated using the Gordon−Taylor equation (eq 1),[48] and the calculated values are lower than the experimentally obtained ones for all polymer/IND ratios. This positive deviation from the theoretical T_g could be attributed to a higher number and strength of interactions between the polymer and the drug in the mixture than in the individual components due to, for example, hydrogen bonding between the amide moieties in the polymer and the carboxylic acid of IND.[49]

Table 2. Thermal Properties of the Neat Polymer and Drug, as well as the Extrudates with Different Polymer/IND Ratios[a]

	T_g^1[°C]	T_g^2[°C]	T_m[°C]	ΔH_f[J g^{-1}]
polymer/IND w/w 1:0	27	27	141	11.84
polymer/IND w/w 2:1	36	32	130	0.75
polymer/IND w/w 1:1	37	35		
polymer/IND w/w 1:2	42	37		
polymer/IND w/w 0:1	43	43	160	108.9

[a] T_g^1 was taken from the second and third heating cycles of DSC measurements (Figure S6). The T_m and ΔH_f were taken from the first heating cycle for IND and from second and third heating cycles for the polymer. T_g^2 was calculated by the Gordon−Taylor equation.

Another method to blend the polymer and the drug via melting could be using a compounder instead of an extruder. In contrast to the presently used extruder and screw set, compounding screw components or a dedicated compounder could potentially lead to improved homogeneity of the blending due to the mechanical mixing of the kneaders or screws for a specific amount of time within the machine setup in addition to the heating of the compounds.

3.3. MEW Printing and Characterization of Scaffolds.

To overcome the remaining crystallinity of IND within the polymer matrix, the DSC measurements showed that simply remelting the extrudates resolved this issue. Apart from the amorphous character, a second parameter is critical to facilitate rapid dissolution—a high surface area. For this, highly porous microfiber meshes consisting of small diameter fibers offer a higher surface area compared to solid films and should be ideal for an accelerated drug release. As mentioned before, MEW has been chosen here to fabricate such controlled microfibrous scaffolds without the use of toxic solvents.

Therefore, the MEW processability of the ABA triblock copolymer, pMeOzi-*b*-pPentOx-*b*-pMeOzi, and the resulting extrudates consisting of different polymer/IND w/w ratios of 2:1, 1:1, and 1:2, were investigated. The neat polymer was processable at a syringe and nozzle temperature of 155 °C. When processing polymer/IND extrudates, with increasing drug content, the processing temperature could be decreased down to 130 °C for the blend containing polymer/IND w/w ratio of 1:2 (Table 1).

Due to the fast solidification of the melts, as previously shown by Nahm et al. for poly(2-ethyl-2-oxazine) (PEtOzi),[50] a small distance of 4 mm between the print head and the collector is required to enable sufficient direct writing. Furthermore, fiber pulsing after 5−10 layers was observed, and therefore, manual adjustment of the applied voltage while printing was needed to enable accurate fiber placement with homogeneous diameters and reduce fiber pulsing or jet break within higher layers.

The resulting fibers exhibit a smooth fiber morphology, and in the case of the neat polymer, a reasonably good stackability and alignment of the MEW fibers (Figure 3) was achieved for 20 layers in each direction, alternating between 0° and 90° fiber orientation while for the different polymer/IND ratios 15 layers in each direction could be printed. All processed polymers and polymer/IND blends show round-shaped fibers

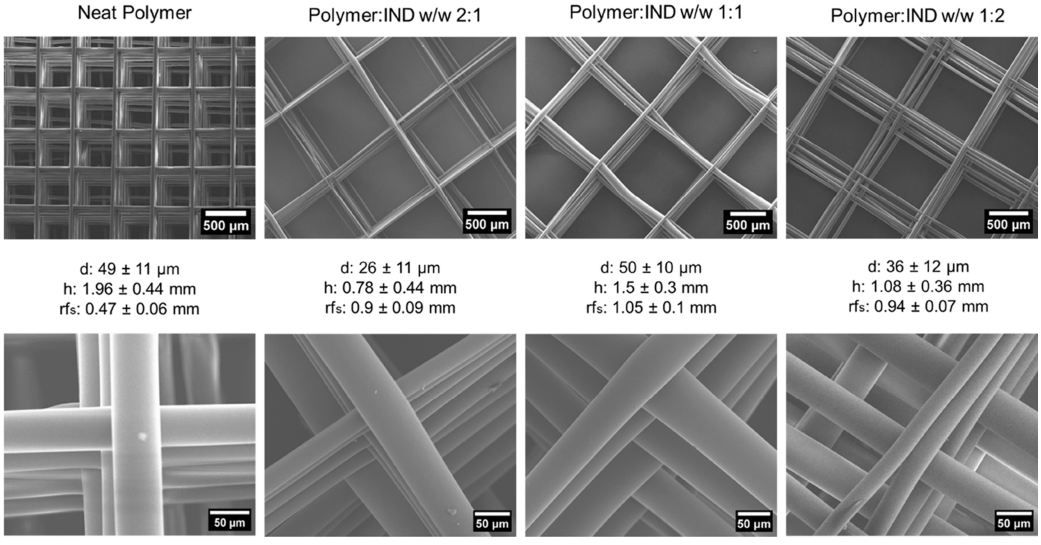

Figure 3. SEM images of the MEW scaffolds fabricated using neat polymer (20 layers; fiber spacing (*fs*) set to 0.5 mm) and different polymer/IND ratios (w/w) of 2:1, 1:1, and 1:2 (15 layers; *fs* set to 1.0 mm), respectively. First row showing overview images, as well as the average fiber diameter (*d*), scaffold height (*h*), and real fiber spacing (*rfs*) results, and second row showing a magnified view, highlighting the smooth fiber surfaces and (sometimes imperfect) stackability of all processed materials.

https://doi.org/10.1021/acsapm.2c01845
ACS Appl. Polym. Mater. 2023, 5, 913−922

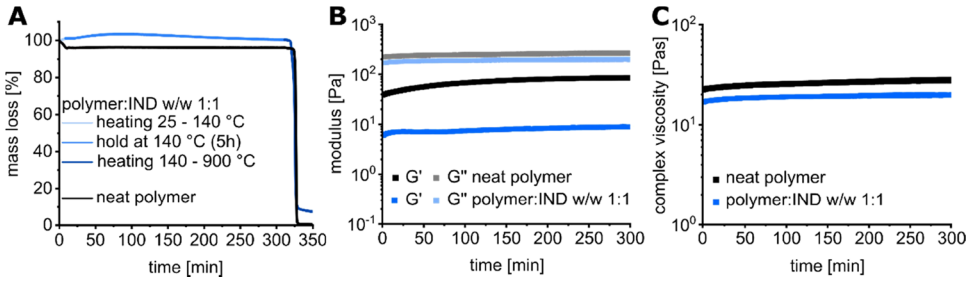

Figure 4. (A) TGA measurement of the neat polymer and the polymer/IND extrudate (w/w) 1:1, (B) rheology time sweep displaying storage modulus G' and loss modulus G'', and (C) rheology time sweep displaying the complex viscosity over the measurement time. Measurements were done at 140 °C for the blend (polymer/IND w/w 1:1) and at 155 °C for the neat polymer.

without noticeable flattening in between the layers. The fiber diameters of all processed materials are between 25 and 50 μm, and the scaffolds heights are between 0.75 and 2 mm (Figure 3). However, no general trend is visible as the printing parameters were individually adjusted for the neat polymer and the polymer/IND blends (Table 1), significantly influencing the resulting fiber diameters. The viscosity of the polymer/IND blends was analyzed by melt rheology measurements at their individual printing temperatures (Figure S7), but also these results show no clear trend that could explain the difference in fiber diameter. By increasing the drug content, the stackability of the fibers deteriorates leading to formation of gaps among the stacked layers. This might be caused by increased electrostatic repulsion between fibers facilitated by the ionizable IND. The distribution of IND in the printed scaffold was investigated by placing the scaffold under UV light, which revealed a homogeneous fluorescence emission (Figure S8).

Using IND as oral capsules or suspension, the drug loading is commonly based on the release rate, age, type, and severity of the patient's condition and is around 20−100 mg per unit.[51] However, in freeze-dried sublingual tablets, the drug loading has been investigated at around 25 mg per unit.[3] When processing the blend polymer/IND 1:2 (w/w) into scaffolds with 15 layers in each direction (0° and 90° fiber orientation), the sample weight is around 90 mg and, therefore, drug loading is about 60 mg, which would be probably sufficient for a single dose. As MEW is a multi-parameter process and the scaffold design is controlled via the G-code, the dosage of IND in MEW-printed scaffolds could be readily adjusted by, for example, changing the fiber diameter as required. The diameter can be varied via the applied pressure and/or the printing speed. Furthermore, the scaffold design can also be altered regarding the fiber spacing and the number of stacked layers resulting in more direct-written material and, respectively, in higher drug-content per volume.

To further improve the layer stacking and scaffold height, a MEW printer with automatically adjustable voltage and Z-height of the print head would be needed, as demonstrated by Wunner and co-workers.[41]

While printing, we observed a color change from yellow to brown of the drug-loaded extrudates over time (Figure S9). IND is known to be easily degradable at elevated temperatures and in particular above its T_m, therefore, a possible degradation was investigated by TGA measurements (Figure 4A). The TGA graph of the polymer showed an initial mass loss of 5% while heating to 140 °C, followed by a plateau during the isotherm.

The initial mass loss could be caused by evaporation of water as the used polymer is hygroscopic and was not dried specifically before the measurement. Increasing the temperature to above 350 °C, degradation of the polymer takes place, as evidenced by the mass loss. A different behavior was observed for the extrudates. During the initial heating process and the isothermal heating, an increase in mass was observed, albeit this mass gain is minor and might be due to oxidation or measuring artifact, as the polymer is expected to be stable up to 350 °C. Similar results have been observed for TGA measurements of MEW-processed samples using PVDF.[34] Further heating to 900 °C resulted in a mass loss from 99 to 9% due to the degradation of the polymer.

The thermal behavior and the resulting potential changes within the polymer/IND extrudates were also investigated by melt rheology (Figure 4B). The value for G'' (loss modulus) was essentially constant at 250 Pa for the neat polymer sample during the whole measurement and at 190 Pa for the polymer/IND extrudate. A slightly different behavior was observed for G' (storage modulus). During heating, a moderate but continuous increase in G' is visible. The increase in elastic strength can be explained by additional molecular entanglement of the polymer chains over time. This effect is more pronounced when measuring the neat polymer. IND reduces the viscosity in the molten blend (Figure 4C), correlating with the decreasing MEW-processing temperatures with increasing drug content (Table 1).[52] Even at a lower printing temperature, the viscosity of the melted blend is lower than that of the neat polymer. Importantly, no major change in viscosity was observed during isothermal heating. Apparently, potential degradation of the drug does not have a marked influence on the viscosity of the blend and, therefore, also not on the printing process. Nevertheless, degradation of the drug after being heated to 140 °C in the printer for several hours could be verified by ^{1}H NMR measurements (Figure S10). A possible degradation mechanism induced by thermal treatment is for instance decarboxylation.[53]

The MEW-printed scaffolds were analyzed by DSC and PXRD to ensure the amorphous state of the drug (Figure 5). As already mentioned before, the signal-to-noise ratio of the PXRD patterns makes it difficult to exclude minute crystalline components, especially since the diffractograms of polymer/IND scaffolds show more noise than those of the neat polymer. However, in contrast to before MEW printing, there is no obvious residual crystallinity left in the structure directly after printing. This could be confirmed by DSC measurements as well. In the first heating curve of the scaffolds, in contrast to before MEW, no melting peak of IND is visible.

https://doi.org/10.1021/acsapm.2c01845
ACS Appl. Polym. Mater. 2023, 5, 913−922

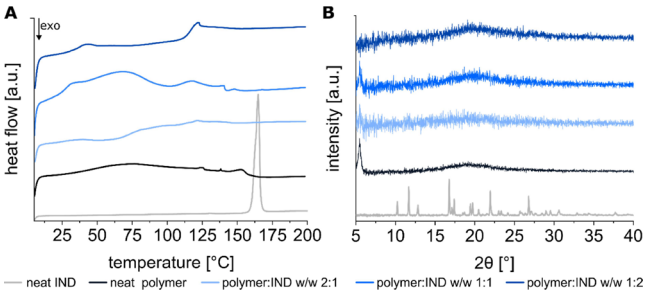

Figure 5. (A) DSC thermograms of MEW-printed scaffolds (first heating) and (B) PXRD pattern of MEW scaffolds fabricated using the neat polymer and polymer/IND blends with ratios (w/w) of 2:1, 1:1, and 1:2, respectively.

After determining the solid-state properties of the drug-loaded scaffolds, their dissolution behavior was investigated. As there is no standardized approach to test the dissolution properties for sublingual dosage forms, the study was done similar to a previously published approach by Lopez and co-workers[54] below the solubility limit of IND in PBS (223 mg mL^{-1}).[55] The MEW-processed scaffolds fabricated using the polymer/IND blends of 2:1, 1:1, and 1:2 (w/w) clearly showed a loading-dependent dissolution behavior (Figure 6).

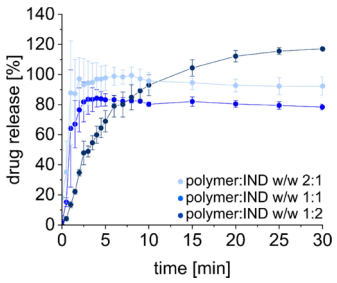

Figure 6. Dissolution profile of the drug-loaded MEW-printed scaffolds (n = 3) with polymer/IND w/w ratios of 2:1, 1:1, and 1:2 in 250 mL of PBS (pH = 7.4).

The samples consisting of polymer/IND 2:1 and 1:1 (w/w), dissolve faster, within about 1 and 2.5 min, and reach a plateau at 95 and 80% released drug, respectively, after which drug concentration stays nearly constant over the remaining experiment duration. In contrast, the scaffolds of polymer/IND 1:2 (w/w) generally show a slower dissolution with finally reaching 120% drug release, even though almost 75% of the drug is released in less than 5 min. We attribute the observation that the final drug release is not 100% as expected to inhomogeneities in the drug content of the individual scaffolds (the average drug content for a batch is determined for different scaffolds compared to those used for the release study). This could potentially be prevented by a more thorough pre-blending using a compounder allowing to also mechanically mix the compounds in contrast to the used extruder setup. This notwithstanding, these dissolution profiles are much faster compared to previous work with different but similar POx-based triblock copolymers and curcumin as the model drug, in which solid pellets were used in dissolution studies. The highest drug loadings, about 1:1, tested in previous work dissolved about 100 times slower than lower drug loadings.[56]

Overall, using the multi-parameter process, i.e., MEW, to process IND-loaded scaffolds for sublingual drug delivery applications enables the fabrication of adaptable patient-specific drug loading.

Although these first MEW-printed drug-loaded scaffolds using an ABA triblock copolymer for sublingual drug application seem to be promising, this method has some limitations. The combination of two high-temperature methods (HME and MEW printing) limits the choice of drug, as it needs to be sufficiently temperature stable. In addition, the total amount of drug that can be printed in suitably sized scaffolds is somewhat limited (here about 60 mg), which makes the use of a relatively potent drug necessary. Additionally, the T_g of the ASD needs to be relatively low to allow printing below the degradation temperature of the drug; in the case presented here, the T_g of the polymer is 27 °C. However, to prevent recrystallization of the drug, a generic rule is that the T_g of the polymer should be around 50 °C above the storage temperature.[57] However, as the long-term stability was not tested within this study, the influence of the low T_g on the recrystallization behavior of the drug, as well as the dissolution behavior of the scaffold after storage, is not clear for the current system. It should be noted that, depending on the viscosity of the melt at a certain temperature, it would be also possible to use polymers with a higher T_g for MEW printing. The critical values that need to be tested in advance are the degradation temperature of the drug and the viscosity of the melt at a certain temperature. A potential limitation of the polymer melt viscosity could be overcome by addition of a plasticizer to decrease the viscosity.

4. CONCLUSIONS

In this study, a highly water-soluble ABA triblock copolymer, comprising 2-methyl-2-oxazine as block A and 2-pentyl-2-oxazoline as block B, was successfully synthesized and blended via HME with IND as the model drug resulting in extrudates with different polymer/IND ratios of 2:1, 1:1, and 1:2 (w/w). Remaining crystallinity after HME of IND within the extrudates was visible but could potentially be removed by optimizing HME parameters. However, the remaining crystallinity resolved during MEW as a 3D printing technology, enabling the fabrication of microfibrous scaffolds with high porosity, and, therefore, large surface area favorable for a fast dissolution of the polymer and drug release. Furthermore, MEW is a multi-parameter process giving the advantage of adjustable scaffold design and, therefore, the drug-loading content within the scaffold.

In summary, this study introduces a new potential polymer excipient enabling amorphous blends with high levels of amorphous drugs for drug delivery applications. Due to the LCROP, the polymer can be easily modulated depending on the requirements. In combination with MEW, highly porous fibrous scaffolds can be fabricated without the need of a toxic solvent and with high precision of fiber placement offering a wide range of designs for further applications, even beyond sublingual drug delivery approaches.

■ ASSOCIATED CONTENT

Supporting Information

The Supporting Information is available free of charge at https://pubs.acs.org/doi/10.1021/acsapm.2c01845.

Detailed information about monomer and polymer synthesis with NMR, SEC, and DSC results, IND standard curve, microscope image of the extrudate, DSC

https://doi.org/10.1021/acsapm.2c01845
ACS Appl. Polym. Mater. 2023, 5, 913−922

thermograms and melt rheology results of polymer/IND blends, pictures of drug-loaded scaffolds under UV light, picture of the sample-loaded syringe showing color change, and NMR indicating partial drug degradation (PDF)

AUTHOR INFORMATION

Corresponding Author

Robert Luxenhofer − *Soft Matter Chemistry, Department of Chemistry, and Helsinki Institute of Sustainability Science, Faculty of Science, University of Helsinki, Helsinki 00014, Finland;* orcid.org/0000-0001-5567-7404; Email: robert.luxenhofer@helsinki.fi

Authors

Larissa Keßler − *Soft Matter Chemistry, Department of Chemistry, and Helsinki Institute of Sustainability Science, Faculty of Science, University of Helsinki, Helsinki 00014, Finland*

Zeynab Mirzaei − *Soft Matter Chemistry, Department of Chemistry, and Helsinki Institute of Sustainability Science, Faculty of Science, University of Helsinki, Helsinki 00014, Finland*

Juliane C. Kade − *Soft Matter Chemistry, Department of Chemistry, and Helsinki Institute of Sustainability Science, Faculty of Science, University of Helsinki, Helsinki 00014, Finland; Polymer Functional Materials, Chair for Advanced Materials Synthesis, Department of Chemistry and Pharmacy, Julius-Maximilians-University Würzburg, Würzburg 97070, Germany; Department for Functional Materials in Medicine and Dentistry at the Institute of Functional Materials and Biofabrication, Julius-Maximilians-University Würzburg, Würzburg 97070, Germany*

Complete contact information is available at: https://pubs.acs.org/10.1021/acsapm.2c01845

Author Contributions

Conceptualization and study design: L.K., Z.M., J.C.K., and R.L. Polymer synthesis and characterization: L.K. Formulation preparation and characterization: L.K., Z.M., and J.C.K. Data acquisition and analysis: L.K., Z.M., and J.C.K. Writing and revising of the manuscript: L.K., Z.M., J.C.K., and R.L. Funding acquisition: R.L. and J.C.K. All authors have read and agreed to the published version of the manuscript.

Notes

The authors declare the following competing financial interest(s): The authors declare the following potential conflicts of interest(s): R.L. is listed as inventors on patents and patent applications pertinent to some materials discussed in this contribution and is co-founder of DelAQUA Pharmaceuticals, intend on commercialization of poly(2-oxazoline) based drug formulations.

ACKNOWLEDGMENTS

The authors would like to gratefully acknowledge the financial support by the Academy of Finland (Grant no. 337660) and Volkswagen Foundation (Grant no. 93418). J.C. Kade is additionally supported by the Joachim Herz Foundation and appreciates financial support from Erasmus+ Traineeship Programme, as well as the Bavarian State Ministry of Science and the Arts and the University of Würzburg to the Graduate School of Life Sciences (GSLS), University of Würzburg, Germany. The authors' grateful thanks are also extended to Prof. Dietmar Hutmacher and Peter Bate for their support in providing the custom-built MEW. Furthermore, the (technical) assistance of Sami-Pekka Hirvonen for SEC, Sami Hietala for melt rheology, and Heikki Räikkönen for PXRD measurements is appreciated.

REFERENCES

(1) Hoffmann, E. M.; Breitenbach, A.; Breitkreutz, J. Advances in orodispersible films for drug delivery. *Expert Opin. Drug Delivery* **2011**, *8*, 299−316.

(2) Li, J. H.; Pan, H.; Ye, Q. Z.; Shi, C. H.; Zhang, X. R.; Pan, W. S. Carvedilol-loaded polyvinylpyrrolidone electrospun nanofiber film for sublingual delivery. *J. Drug Delivery Sci. Technol.* **2020**, *58*, 101726−101733.

(3) Ibrahim, M. S.; Elmahdy Elsayyad, N. M.; Salama, A.; Noshi, S. H. Quality by Design (Qbd) as a Tool for the Optimization of Indomethacin Freeze-Dried Sublingual Tablets: In Vitro and in Vivo Evaluation. *Int. J. Appl. Pharm.* **2021**, *13*, 160−171.

(4) Labhade, S.; Malode, C.; Rawal, V.; Rupvate, S. Review on Sublingual Drug Delivery System. *J. Drug Delivery Ther.* **2019**, *9*, 684−688.

(5) Maity, B.; Chatterjee, A.; Ahmed, S. A.; Seth, D. Interaction of the nonsteroidal anti-inflammatory drug indomethacin with micelles and its release. *J. Phys. Chem. B* **2015**, *119*, 3776−3785.

(6) Gliszczynska, A.; Nowaczyk, M. Lipid Formulations and Bioconjugation Strategies for Indomethacin Therapeutic Advances. *Molecules* **2021**, *26*, 1576−1594.

(7) Hu, C.; Zhang, F.; Fan, H. Evaluation of Drug Dissolution Rate in Co-amorphous and Co-crystal Binary Drug Delivery Systems by Thermodynamic and Kinetic Methods. *AAPS PharmSciTech* **2021**, *22*, 21−30.

(8) Moseson, D. E.; Parker, A. S.; Beaudoin, S. P.; Taylor, L. S. Amorphous solid dispersions containing residual crystallinity: Influence of seed properties and polymer adsorption on dissolution performance. *Eur. J. Pharm. Sci.* **2020**, *146*, 105276−105288.

(9) Bhujbal, S. V.; Mitra, B.; Jain, U.; Gong, Y.; Agrawal, A.; Karki, S.; Taylor, L. S.; Kumar, S.; Tony Zhou, Q. Pharmaceutical amorphous solid dispersion: A review of manufacturing strategies. *Acta Pharm. Sin. B* **2021**, *11*, 2505−2536.

(10) Jelić, D.; Liavitskaya, T.; Vyazovkin, S. Thermal stability of indomethacin increases with the amount of polyvinylpyrrolidone in solid dispersion. *Thermochim. Acta* **2019**, *676*, 172−176.

(11) Browne, E.; Worku, Z. A.; Healy, A. M. Physicochemical Properties of Poly-Vinyl Polymers and Their Influence on Ketoprofen Amorphous Solid Dispersion Performance: A Polymer Selection Case Study. *Pharmaceutics* **2020**, *12*, 433−456.

(12) Feng, S.; Bandari, S.; Repka, M. A. Investigation of poly(2-ethyl-2-oxazoline) as a novel extended release polymer for hot-melt extrusion paired with fused deposition modeling 3D printing. *J. Drug Delivery Sci. Technol.* **2022**, *74*, No. 103558.

(13) Fael, H.; Rafols, C.; Demirel, A. L. Poly(2-Ethyl-2-Oxazoline) as an Alternative to Poly(Vinylpyrrolidone) in Solid Dispersions for Solubility and Dissolution Rate Enhancement of Drugs. *J. Pharm. Sci.* **2018**, *107*, 2428−2438.

(14) Edueng, K.; Mahlin, D.; Bergstrom, C. A. S. The Need for Restructuring the Disordered Science of Amorphous Drug Formulations. *Pharm. Res.* **2017**, *34*, 1754−1772.

(15) Lübtow, M. M.; Keßler, L.; Appelt-Menzel, A.; Lorson, T.; Gangloff, N.; Kirsch, M.; Dahms, S.; Luxenhofer, R. More Is Sometimes Less: Curcumin and Paclitaxel Formulations Using Poly(2-oxazoline) and Poly(2-oxazine)-Based Amphiphiles Bearing Linear and Branched C9 Side Chains. *Macromol. Biosci.* **2018**, *18*, 1800155−1800172.

(16) Haider, M. S.; Luxenhofer, R. Development of Poly(2-oxazoline) s and poly(2-oxazine) s based formulation library and estimation of polymer/drug compatibility. *ChemRxiv* **2022**, DOI: 10.26434/chemrxiv-2022-s8xc3.

(17) Lübtow, M. M.; Lorson, T.; Finger, T.; Gröber-Becker, F. K.; Luxenhofer, R. Combining Ultra-High Drug-Loaded Micelles and Injectable Hydrogel Drug Depots for Prolonged Drug Release. *Macromol. Chem. Phys.* **2019**, *221*, 1900341−1900354.
(18) Luxenhofer, R.; Sahay, G.; Schulz, A.; Alakhova, D.; Bronich, T. K.; Jordan, R.; Kabanov, A. V. Structure-property relationship in cytotoxicity and cell uptake of poly(2-oxazoline) amphiphiles. *J. Controlled Release* **2011**, *153*, 73−82.
(19) Seo, Y.; Schulz, A.; Han, Y. C.; He, Z. J.; Bludau, H.; Wan, X. M.; Tong, J.; Bronich, T. K.; Sokolsky, M.; Luxenhofer, R.; Jordan, R.; Kabanov, A. V. Poly(2-oxazoline) block copolymer based formulations of taxanes: effect of copolymer and drug structure, concentration, and environmental factors. *Polym. Adv. Technol.* **2015**, *26*, 837−850.
(20) Sedlacek, O.; Bardoula, V.; Vuorimaa-Laukkanen, E.; Gedda, L.; Edwards, K.; Radulescu, A.; Mun, G. A.; Guo, Y.; Zhou, J.; Zhang, H.; Nardello-Rataj, V.; Filippov, S.; Hoogenboom, R. Influence of Chain Length of Gradient and Block Copoly(2-oxazoline)s on Self-Assembly and Drug Encapsulation. *Small* **2022**, *18*, 2106251−2106261.
(21) Sedlacek, O.; Hoogenboom, R. Drug Delivery Systems Based on Poly(2-Oxazoline)s and Poly(2-Oxazine)s. *Adv. Ther.* **2019**, *3*, 1900168−1900186.
(22) Vlassi, E.; Papagiannopoulos, A.; Pispas, S. Amphiphilic poly(2-oxazoline) copolymers as self-assembled carriers for drug delivery applications. *Eur. Polym. J.* **2017**, *88*, 516−523.
(23) Luxenhofer, R.; Schulz, A.; Roques, C.; Li, S.; Bronich, T. K.; Batrakova, E. V.; Jordan, R.; Kabanov, A. V. Doubly amphiphilic poly(2-oxazoline)s as high-capacity delivery systems for hydrophobic drugs. *Biomaterials* **2010**, *31*, 4972−4979.
(24) Zahoranova, A.; Luxenhofer, R. Poly(2-oxazoline)- and Poly(2-oxazine)-Based Self-Assemblies, Polyplexes, and Drug Nanoformulations-An Update. *Adv. Healthcare Mater.* **2021**, *10*, 2001382−2001409.
(25) Chroni, A.; Mavromoustakos, T.; Pispas, S. Poly(2-oxazoline)-Based Amphiphilic Gradient Copolymers as Nanocarriers for Losartan: Insights into Drug−Polymer Interactions. *Macromolecules* **2021**, *1*, 177−200.
(26) Anane-Adjei, A. B.; Jacobs, E.; Nash, S. C.; Askin, S.; Soundararajan, R.; Kyobula, M.; Booth, J.; Campbell, A. Amorphous solid dispersions: Utilization and challenges in preclinical drug development within AstraZeneca. *Int. J. Pharm.* **2022**, *614*, 121387−121403.
(27) Modica de Mohac, L.; Keating, A. V.; de Fatima Pina, M.; Raimi-Abraham, B. T. Engineering of Nanofibrous Amorphous and Crystalline Solid Dispersions for Oral Drug Delivery. *Pharmaceutics* **2019**, *11*, 7.
(28) Davoodi, P.; Lee, L. Y.; Xu, Q.; Sunil, V.; Sun, Y.; Soh, S.; Wang, C. H. Drug delivery systems for programmed and on-demand release. *Adv. Drug Delivery Rev.* **2018**, *132*, 104−138.
(29) Qi, S.; Craig, D. Recent developments in micro- and nanofabrication techniques for the preparation of amorphous pharmaceutical dosage forms. *Adv. Drug Delivery Rev.* **2016**, *100*, 67−84.
(30) Saidy, N. T.; Fernández-Colino, A.; Heidari, B. S.; Kent, R.; Vernon, M.; Bas, O.; Mulderrig, S.; Lubig, A.; Rodríguez-Cabello, J. C.; Doyle, B.; Hutmacher, D. W.; De-Juan-Pardo, E. M.; Mela, P. Spatially Heterogeneous Tubular Scaffolds for In Situ Heart Valve Tissue Engineering Using Melt Electrowriting. *Adv. Funct. Mater.* **2022**, *32*, No. 2110716.
(31) Kade, J. C.; Dalton, P. D. Polymers for Melt Electrowriting. *Adv. Healthcare Mater.* **2021**, *10*, 2001232−2001250.
(32) Robinson, T. M.; Hutmacher, D. W.; Dalton, P. D. The Next Frontier in Melt Electrospinning: Taming the Jet. *Adv. Funct. Mater.* **2019**, *29*, 1904664−1904692.
(33) Mondadori, C.; Chandrakar, A.; Lopa, S.; Wieringa, P.; Talo, G.; Perego, S.; Lombardi, G.; Colombini, A.; Moretti, M.; Moroni, L. Assessing the response of human primary macrophages to defined fibrous architectures fabricated by melt electrowriting. *Bioact. Mater.* **2023**, *21*, 209−222.
(34) Florczak, S.; Lorson, T.; Zheng, T.; Mrlik, M.; Hutmacher, D. W.; Higgins, M. J.; Luxenhofer, R.; Dalton, P. D. Melt electrowriting of electroactive poly(vinylidene difluoride) fibers. *Polym. Int.* **2019**, *68*, 735−745.
(35) Youssef, A.; Hrynevich, A.; Fladeland, L.; Balles, A.; Groll, J.; Dalton, P. D.; Zabler, S. The Impact of Melt Electrowritten Scaffold Design on Porosity Determined by X-Ray Microtomography. *Tissue Eng., Part C* **2019**, *25*, 367−379.
(36) Meng, J.; Boschetto, F.; Yagi, S.; Marin, E.; Adachi, T.; Chen, X. F.; Pezzotti, G.; Sakurai, S.; Yamane, H.; Xu, H. Z. Design and manufacturing of 3D high-precision micro-fibrous poly (L-lactic acid) scaffold using melt electrowriting technique for bone tissue engineering. *Mater. Des.* **2021**, *210*, 110063−110072.
(37) Su, Y.; Muller, C. A.; Xiong, X.; Dong, M.; Chen, M. Reshapable Osteogenic Biomaterials Combining Flexible Melt Electrowritten Organic Fibers with Inorganic Bioceramics. *Nano Lett.* **2022**, *22*, 3583−3590.
(38) Bai, J.; Wang, H.; Gao, W.; Liang, F.; Wang, Z.; Zhou, Y.; Lan, X.; Chen, X.; Cai, N.; Huang, W.; Tang, Y. Melt electrohydrodynamic 3D printed poly (epsilon-caprolactone)/polyethylene glycol/roxithromycin scaffold as a potential anti-infective implant in bone repair. *Int. J. Pharm.* **2020**, *576*, 118941−118950.
(39) Witte, H.; Seeliger, W. Simple Synthesis of 2-Substituted 2-Oxazolines and 5,6-Dihydro-4h-1,3-Oxazines. *Angew. Chem., Int. Ed.* **1972**, *11*, 287−288.
(40) Lubtow, M. M.; Hahn, L.; Haider, M. S.; Luxenhofer, R. Drug Specificity, Synergy and Antagonism in Ultrahigh Capacity Poly(2-oxazoline)/Poly(2-oxazine) based Formulations. *J. Am. Chem. Soc.* **2017**, *139*, 10980−10983.
(41) Wunner, F. M.; Bas, O.; Saidy, N. T.; Dalton, P. D.; Pardo, E. M. D.; Hutmacher, D. W. Melt Electrospinning Writing of Three-dimensional Poly(epsilon-caprolactone) Scaffolds with Controllable Morphologies for Tissue Engineering Applications. *J. Visualized Exp.* **2017**, *130*, 56289−56301.
(42) Schindelin, J.; Arganda-Carreras, I.; Frise, E.; Kaynig, V.; Longair, M.; Pietzsch, T.; Preibisch, S.; Rueden, C.; Saalfeld, S.; Schmid, B.; Tinevez, J. Y.; White, D. J.; Hartenstein, V.; Eliceiri, K.; Tomancak, P.; Cardona, A. Fiji: an open-source platform for biological-image analysis. *Nat. Methods* **2012**, *9*, 676−682.
(43) Sedlacek, O.; Lava, K.; Verbraeken, B.; Kasmi, S.; De Geest, B. G.; Hoogenboom, R. Unexpected Reactivity Switch in the Statistical Copolymerization of 2-Oxazolines and 2-Oxazines Enabling the One-Step Synthesis of Amphiphilic Gradient Copolymers. *J. Am. Chem. Soc.* **2019**, *141*, 9617−9622.
(44) Saegusa, T.; Kobayashi, S.; Nagura, Y. Isomerization polymerization of 1,3-oxazine. IV. Kinetic studies on the polymerization of 2-methyl-5,6-dihydro-4H-1,3-oxazine. *Macromolecules* **1974**, *7*, 713−716.
(45) Wu, Y.; Hu, J. L.; Zhang, C.; Han, J.; Wang, Y.; Kumar, B. A facile approach to fabricate a UV/heat dual-responsive triple shape memory polymer. *J. Mater. Chem. A* **2015**, *3*, 97−100.
(46) Huang, D.; Xie, Z.; Rao, Q.; Liamas, E.; Pan, P.; Guan, S.; Zhang, Z. J.; Lu, M.; Li, Q. Hot melt extrusion of heat-sensitive and high melting point drug: Inhibit the recrystallization of the prepared amorphous drug during extrusion to improve the bioavailability. *Int. J. Pharm.* **2019**, *565*, 316−324.
(47) S'Ari, M.; Blade, H.; Cosgrove, S.; Drummond-Brydson, R.; Hondow, N.; Hughes, L. P.; Brown, A. Characterization of Amorphous Solid Dispersions and Identification of Low Levels of Crystallinity by Transmission Electron Microscopy. *Mol. Pharmaceutics* **2021**, *18*, 1905−1919.
(48) Mahieu, A.; Willart, J. F.; Dudognon, E.; Danede, F.; Descamps, M. A new protocol to determine the solubility of drugs into polymer matrixes. *Mol. Pharmaceutics* **2013**, *10*, 560−566.
(49) Gupta, P.; Bansal, A. K. Molecular interactions in celecoxib-PVP-meglumine amorphous system. *J. Pharm. Pharmacol.* **2005**, *57*, 303−310.

https://doi.org/10.1021/acsapm.2c01845
ACS Appl. Polym. Mater. 2023, 5, 913−922

(50) Nahm, D.; Weigl, F.; Schafer, N.; Sancho, A.; Frank, A.; Groll, J.; Villmann, C.; Schmidt, H. W.; Dalton, P. D.; Luxenhofer, R. A versatile biomaterial ink platform for the melt electrowriting of chemically-crosslinked hydrogels. *Mater. Horiz.* **2020**, *7*, 928−933.
(51) Li, J.; Li, L. B.; Nessah, N.; Huang, Y.; Hidalgo, C.; Owen, A.; Hidalgo, I. J. Simultaneous Analysis of Dissolution and Permeation Profiles of Nanosized and Microsized Formulations of Indomethacin Using the In Vitro Dissolution Absorption System 2. *J. Pharm. Sci.* **2019**, *108*, 2334−2340.
(52) Böhm, C.; Tandon, B.; Hrynevich, A.; Teßmar, J.; Dalton, P. D. Processing of Poly(lactic-co-glycolic acid) Microfibers via Melt Electrowriting. *Macromol. Chem. Phys.* **2022**, *223*, No. 2100417.
(53) Shimada, Y.; Komaki, H.; Hirai, A.; Goto, S.; Hashimoto, Y.; Uchiro, H.; Terada, H. Decarboxylation of indomethacin induced by heat treatment. *Int. J. Pharm.* **2018**, *545*, 51−56.
(54) Lopez, F. L.; Shearman, G. C.; Gaisford, S.; Williams, G. R. Amorphous formulations of indomethacin and griseofulvin prepared by electrospinning. *Mol. Pharmaceutics* **2014**, *11*, 4327−4338.
(55) El-Badry, M.; Fetih, G.; Fathy, M. Improvement of solubility and dissolution rate of indomethacin by solid dispersions in Gelucire 50/13 and PEG4000. *Saudi Pharm. J.* **2009**, *17*, 217−225.
(56) Pöppler, A. C.; Lubtow, M. M.; Schlauersbach, J.; Wiest, J.; Meinel, L.; Luxenhofer, R. Loading-Dependent Structural Model of Polymeric Micelles Encapsulating Curcumin by Solid-State NMR Spectroscopy. *Angew. Chem., Int. Ed.* **2019**, *58*, 18540−18546.
(57) Jelic, D. Thermal Stability of Amorphous Solid Dispersions. *Molecules* **2021**, *26*, 238.

https://doi.org/10.1021/acsapm.2c01845
ACS Appl. Polym. Mater. 2023, 5, 913−922